View metadata, citation and similar papers at core.ac.uk
brought to you by CORE
provided by Archivio istituzionale della ricerca - Università di Trieste

The ionic states of iodobenzene studied by photoionization and *ab initio* configuration interaction and DFT computations

Michael H. Palmer,[1] Trevor Ridley,[1] Søren Vrønning Hoffmann,[2] Nykola C. Jones,[2] Marcello Coreno,[3] Monica de Simone,[4] Cesare Grazioli,[4,5] Malgorzata Biczysko,[6,7] and Alberto Baiardi[7]

[1] *School of Chemistry, University of Edinburgh, Joseph Black Building, David Brewster Road, Edinburgh EH9 3FJ, Scotland, UK*

[2] *ISA, Department of Physics and Astronomy, Aarhus University, Ny Munkegade 120, DK-8000 Aarhus C, Denmark*

[3] *CNR-IMIP, Montelibretti, c/o Laboratorio Elettra, Trieste, Italy*

[4] *CNR-IOM Laboratorio TASC, Trieste, Italy*

[5] *Department of Chemical and Pharmaceutical Sciences, University of Trieste, Italy*

[6] *National Research Council ICCOM-CNR, UOS di Pisa, Via G. Moruzzi 1, I-56124 Pisa, Italy*

[7] *Scuola Normale Superiore, Piazza Cavalieri 7, 56126 Pisa, Italy*

Email: *m.h.palmer@ed.ac.uk; tr01@staffmail.ed.ac.uk; vronning@phys.au.dk; nykj@phys.au.dk; marcello.coreno@elettra.eu; desimone@iom.cnr.it*; *malgorzata.biczysko@sns.it*

Phone[a]: +44 (0) 131 650 4822

ABSTRACT

New valence electron photoelectron spectra of iodobenzene obtained using synchrotron radiation have been recorded. Ionization energies (IE) determined using multi-configuration SCF calculations (MCSCF) procedures confirmed the adiabatic IE order as: $X^2B_1 < A^2A_2 < B^2B_2 < C^2B_1$. Although it is convenient to retain C_{2v} labelling, there is evidence that minor distortion to C_S symmetry occurs at the MCSCF level for the C state. The fifth ionization process shown to be D^2A_1, exhibits dissociation to $C_6H_5^+ + I$, both in the experimental and theoretical studies. The calculated Franck-Condon vibrational spectral envelopes, including hot band contributions, for the first four ionic states reproduce the observed peak positions and intensities with reasonable accuracy. In order to simulate the

observed spectra, characteristic bandwidths are required. The increase in the required bandwidths for the A^2A_2 and B^2B_2 states is attributed to internal conversion to lower-lying states. The presence of relatively high intensity sequence bands, leads to asymmetry of each of the X^2B_1 state bands.

1. INTRODUCTION

In this paper, we present new high-resolution, synchrotron- excited photoelectron spectra (PES) and, in the accompanying paper (AP),[1] 1-photon, vacuum ultraviolet (VUV) absorption spectra of iodobenzene (***PhI***), both at room temperature.

In several respects, the spectra of ***PhI*** are the most complex of the monohalobenzenes (C_6H_5I, C_6H_5Br, C_6H_5Cl, and C6H5F, "the series," ***PhX***), and are difficult to interpret in isolation. We will be presenting similar studies of the lower members of the ***PhX*** series later, where we will also present (2 + 1) and (3 + 1) resonance enhanced multiphoton ionization (REMPI) spectra of jet-cooled samples. The present analyses of the PES (and VUV spectra) are supported by ab initio configuration interaction (CI) and time dependent density functional (TDDFT) calculations of vertical and adiabatic ionization (and excitation) energies. The Franck-Condon (FC) vibrational profiles of both hot and cold bands of these ionized (and excited states) are analyzed in detail for the first time.

We will begin Sec. III by giving an overview of the PES and VUV spectra of all four molecules which, as well as being of interest in themselves and demonstrating trends in ionization energy (IE) with halogen, will provide a model for the subsequent papers. PES are important for identification of Rydberg states in the VUV absorption spectrum, since the potentials experienced in the ionic (PES) and Rydberg state (VUV) formation, particularly for high-n states, are similar and this leads to similar vibrational profiles in the two types of spectra.[2–8] Therefore, in the analysis of the absorption spectra in the AP,[1] we use the vibronic structure observed in the PES as a fingerprint to identify the ionic core of the observed Rydberg state or series. Hence, it is essential to have a detailed knowledge of the PES themselves. The current VUV energy range goes up to 11 eV approximately and in this range for ***PhI***, all the first four ionic state band systems are relevant; these have relatively similar intensities in the PES but in addition, three of the IE clearly overlap, leading to potential overlap of the Rydberg state profiles, as is discussed in the AP.[1] Consequently, in the VUV spectra, the Rydberg series converging on these ionization limits also overlap making assignment of the spectra more difficult.

The value of the first ionization energy, IE1, for ***PhI*** has been obtained using various techniques.[9–12] The most accurate value of 70 638 ± 5 cm^{-1} (8.7580(7) eV)was obtained from the 1-photon VUV laser-excited mass analyzed threshold ionization (MATI) spectrum,[12] while the most accurate HeI-excited PES value reported was 70 605 cm^{-1} (8.754 eV).[11]

The higher states of the ion, together with those of PhCl and PhBr, have been studied in detail by Holland et al.[11,13,14] using synchrotron- and HeI-excited PES. In the present program of studies, we have re-recorded the synchrotron-excited spectra with extra sensitivity and resolution and have recorded a high-resolution spectrum of PhF for the first time. Although our interpretations are broadly in agreement with those reported, [11,13,14] our calculations of the relevant Franck-Condon factors (FCF) show that the spectra are more complex than previously suggested, with many of the observed peaks having more than one component band, on both leading and trailing energy sides. The calculated FCFs for the ground state of the ion will also be compared with the intensities of the bands in thematic spectrum.[12] Overall, we aim to give a more global view of the PES, particularly in terms of the vibrational structure, identifying trends in the spectra as the mass of the halogen changes.

In the PES discussion below, our units for the overview spectrum and for electronic origins are electron volts (eV), which enables more easy comparison with previous work; but when discussing individual PES bands and vibrational frequencies, we use units of cm^{-1}, since these are more closely aligned with the VUV studies of Rydberg states. The vibrational modes, numbered according to the Mulliken convention, are shown in Table I. For the ***PhX*** series, modes 1-11 have a1 symmetry and are numbered in descending order of frequencies; only these modes are observed as cold bands in the PES.

II. EXPERIMENTAL AND COMPUTATIONAL PROCEDURES

A. Experimental

ThePES for ***PhI*** (CAS Registry Number 591-50-4, Sigma- Aldrich) were measured at the gas phase photoemission beamline[16] at the Elettra synchrotron radiation laboratory in Trieste, Italy. Undulator radiation in the photon range of 14–900 eV was monochromatized by a spherical grating monochromator, equipped with a planar pre-mirror and five interchangeable gratings. Electron spectra were measured using the original SES-200 electron analyzer,[17] mounted at the magic angle (54.7°) with respect to the electric vector of the linearly polarized incident light.With the use of this angle, angle-integrated electron spectra could be obtained. Very high resolution data could be recorded by using the high pressure gas cell (SCIENTA™). In particular, for data acquired with a photon energy of 30 eV over the binding energy range 8.1-12.0 eV (step 1 meV), the overall experimental energy resolution was ~8 meV. The energy scale of the PES has been calibrated using the sample gases lines: Ar 3p, Xe

5p, and Xe 4d.[18–20] In this way, we also checked the linearity of the kinetic energy scale of the electron analyzer. Intensities between PES bands are not relevant here, but internal differences are important for Rydberg state analysis. Therefore, the PES have not been corrected for the response function of the detector.

The low-energy region containing the four lowest IEs, IE1-4, which are relevant to the current VUV spectral analysis is shown in Fig. 1. The IEs were measured by fitting to sets of Gaussian functions. A wide scan spectrum recorded for the range 8-32 eV was obtained using 95 eV photons with an overall experimental energy resolution of 25 meV; detailed discussion of this spectrum and its theoretical correlation is deferred to in the supplementary material (S1).[21]

The VUV absorption spectra were measured on the ASTRID2 storage ring at Aarhus University, Denmark, using the AU-UV beam line. Full details are given in the AP.[1]

B. Computational methods

The C_{2v}, ***PhI*** molecule lies in the yz-plane, with the C_2 axis along the z-axis. The adiabatic excitation energies of several low-lying ionic (and singlet states), with their corresponding structures, were obtained using the multiconfiguration SCF calculations (MCSCF) state-averaged (SA) method in MOLPRO,[22] as well as the unrestricted Hartree- Fock (UHF) calculations of GAUSSIAN-09.[23]

Our computation of vibronic spectra used the general approach proposed by Barone et al.[24–27] and implemented in GAUSSIAN-09.[23] This method relies on the Born–Oppenheimer approximation (and on the Eckart conditions) and supports both the time-independent and time-dependent quantum mechanical approaches, and is described in more detail in Refs. 24, 27, and 28. Here, we apply the time-independent FC Adiabatic-Hessian (FCAH) procedure.[24,27] The equilibrium structures, force constants, and vibrational frequencies of each of the neutral ground state and of the ionic states are combined to compute the overlap integrals between the vibrational wave functions of the initial and final electronic states, yielding the intensity of specific vibronic transitions. The normal coordinates of the final (upper) state are expressed in terms of the normal coordinates of the initial (lower) state, using the linear transformation, $Q^I = JQ^F + K$; here, J is the so-called Duschinsky matrix[29] and represents the mixing of the normal modes during the transition and K represents the geometry shift between the initial and final states expressed in terms of the normal modes of the initial state. Q^I and Q^F represent the normal coordinates of the initial and final states, respectively.

The Duschinsky matrix used to derive anharmonic corrections in the excited (ionic) states[25] is based on anharmonic computations for the ground state, where the latter are performed within second-order vibrational perturbation theory (VPT2).[30]

The anharmonic vibrational frequencies for the X^1A_1 state were obtained by means of hybrid models where the harmonic part is computed with larger basis sets or at a higher level of theory with respect to the calculation of the anharmonic correction.[31] In this case, the harmonic frequencies computed using the CAM-B3LYP functional and the Sadlej[32] p-VTZ basis set were combined with anharmonic corrections computed at B3LYP/SNSD level (see below). Finally, temperature effects were introduced by including transitions from vibrationally excited levels of the electronic ground state.[27] In the time independent approach, each vibrational state with a Boltzmann population higher than 0.1% of that of the vibrational ground state has been considered.[27]

The calculated anharmonic values for various states of the ion are presented in Table I. C_{2v} symmetry was maintained for calculations on the X^2B_1, A^2A_2, B^2B_2, and C^2B_1 states at the equilibrium structural searches; in all cases, the Duschinsky matrices are nearly diagonal showing that only a very few normal coordinates of the ion involve significant mode mixing of those for the neutral ground state that have the same symmetry: these are highlighted in Table I. C_1 symmetry was used for the MCSCF frequency calculation on the C^2B_1 state, a necessary feature of the MOLPRO suite; this enabled potential mixing of modes of different symmetries, but all these modes could be easily projected to C_{2v} ones; vibrations affected are also highlighted in Table I.

C. Basis sets and CI study.

Here, we summarize the procedures and further details are given in the supplementary material (S2).[21] We found that the best spectral interpretation was obtained using triple-ζ valence shell (TZV) with polarization (P) bases, and specifically Sadlej[32] p-VTZ I atom basis set ([11s8p6d2f] contracted functions) in combination with the C and H atom bases TZVP[33] and aug-cc-pVTZ.[34] In addition, to generate anharmonic corrections to frequencies and intensities, we used the double-ζ SNSD basis set[35] in conjunction with the B3LYP functional, previously successful for a series of halogenated organic compounds.[36]

In the CI methods, 29 core orbitals ($15a_1 + 5b_1 + 7b_2 + 2a_2$) are omitted; the full valence shell occupied orbitals ($8a_1 + 3b_1 + 6b2 + 1a_2$) were used, together with up to 120 virtual MOs (VMOs). Valence shell numbering is generally used for ionic states, in order to facilitate comparisons with the lower ***PhX*** series; however, all-electron numbering is occasionally used

to facilitate comparison with the ground state numbering and some earlier published work. Variations in state structural details are discussed in the supplementary material (S3),[21] but the structures of states of particular importance to the PES study are discussed below.

III. RESULTS

A. Overall aspects

Overviews of the PES spectra of the four ***PhX*** molecules are shown in Fig. 2. In all cases, the X^2B_1 and A^2A_2 states are derived from the splitting of the degenerate $^2E_{1g}$ benzene state by the halogen atom. In PhCl, PhBr, and ***PhI***, the B and C states have been assigned as $^2B_2$ and $^2B_1$ states, respectively, which largely result from the removal of lone pair electrons on the halogen [11,13,14] (in-plane and out-of-plane, respectively). In subsequent papers, we will discuss the symmetry of the B states in PhCl and PhF in more detail. The electron density contours for the four highest occupied MOs of ***PhI*** are shown in Fig. 3. It can be seen that the binding energy of the B state decreases significantly as the mass of the halogen increases until, in ***PhI***, it overlaps the high-energy region of the A^2A_2 state resulting in, as we will discuss later, internal conversion (IC) to the A^2A_2 state. In the PES of PhCl and PhBr, the B state band stands out as most of its intensity is contained in the narrow origin band with very little in the associated vibrational structure. In ***PhI***, IC both greatly diminishes the relative intensity of and increases the width of the origin of the B state band, as shown in Fig. 2, causing it to be less dominant.

It is the peak intensity of the band that is diminished and this is a result of the increased width of the features. This effect carries over to the VUV absorption spectra, where Rydberg states with a B state ionic core stand out in the spectra of PhCl and PhBr but are barely observable in the spectrum of ***PhI***. This is demonstrated for the 3s Rydberg states, [3]3s, highlighted in Fig. 4, where [3] indicates a Rydberg state with a third lowest, B ionization limit; this is discussed further in the AP.[1] In this situation, the bands converging to the B state are very broad; it is their lower peak intensity that makes them difficult to observe and not their inherent weakness.

B. The equilibrium structures of the ionized states of *PhI*

The equilibrium structures for the four lowest ionic states, determined by MCSCF methods, are shown in the supplementary material (S3).21 The geometries of the X^2B_1 ($3b^{-1}_1$) and A^2A_2 ($1a^{-1}_2$) states are almost unchanged from that of the neutral ground state. The B^2B_2 ($6b^{-1}_2$) state shows some C–I bond lengthening (+0.07 Å). These relatively small differences from the neutral ground state are consistent with an intense origin band in the PES. In contrast, theC^2B_1 ($2b_1^{-1}$) state shows greater differences from the lower ionic states, with substantial lengthening of the C_2C_3 and C_5C_6 bonds in what is still a C_{2V} structure. Equilibrium structures computed with smaller basis sets show minor distortion to C_S symmetry. However, these bond differences have only a minor effect on the PES where we still observe an intense origin band. The D^2A_1 state dissociates to $C_6H_5^+$ + I in both the MCSCF (restricted Hartree-Fock) and UB3LYP (unrestricted Hartree-Fock) methods.

C. A comparison of the PES data with the theoretical study

We have used the Tamm-Dancoff approximation (TDA) procedure to determine the higher PES ionic state symmetry sequence for ***PhI*** and the relative intensity profile; a comparison with previous results is given in the supplementary material (S1).[21]

The experimental adiabatic ionization energies IE_1 to IE_4 together with those calculated using UB3LYP and MCSCF and vertical IEs calculated using the Green's Function (GF) (for the outer valence shell ionization) are shown in Table II.

Although the symmetry sequence of IEs calculated by the MCSCF and UB3LYP is the same, the UHF energy differences between adjacent IEs are in closer agreement with experiment.

The adiabatic IEs in the MCSCF calculations are low for each state by almost 1 eV. A probable reason is the inability of obtaining balanced electron correlation between ground and ionized states; this is exemplified by the X^1A_1 state (20 active electrons) and X^2B_1 state (19 electrons), which generate 16×10^6 and 22×10^6 determinants, under the same active set conditions (16 active orbitals). The vibrational frequencies obtained with these structures were combined with the FCAH methodology to determine the vibrational profiles of the ionized state, as described below.

D. Vibrational analysis of the PES spectrum

The PES of the ionic states relevant to the Rydberg states seen in the VUV absorption spectrum, ($IE_{1\text{-}4}$), are comparable with those recorded earlier with HeI (21.2 eV) irradiation,[11] but show much higher counts in the new data. In addition, although the resolution of the spectrometers used in the current and previous studies[11] are both nominally ~8 meV, it appears that the present spectra are slightly more resolved as can be seen from a comparison of the C^2B_1 bands in the two PES. The measured peak positions, their separations from the electronic origins, and their assignments based on the FCF calculations are shown in Table III. A table of the calculated frequencies of the vibrations in the ionic states principally observed in the PES, together with calculated transition intensities, is given in the supplementary material (S4).[21]

1. The X^2B_1 band

The X^2B_1 ($3b_1^{-1}$) band of the PES of ***PhI*** and a stick spectrum of the calculated FCFs are shown in Figs. 5(b) and 5(a), respectively. The experimental spectrum is dominated by a progression of ν_{11} (280 cm^{-1}), with v = 0-4, built on the electronic origin. The same progression built on a band at +1032 cm^{-1} is also observed. Our calculations show that the major assignment of this band is to one quantum of ν_7 (1060 cm^{-1}), as previously reported,[11] but that there is a minor contribution from one quantum of ν_9 (1004 cm^{-1}).

Similarly, it is calculated that one quantum of ν_4 (1596 cm^{-1}) makes a contribution to the peak previously labelled $7^1 11^2$.[11]

The simulation of the total X2B1 band obtained by convoluting the full stick spectrum, including hot bands, (shown in Fig. 5(a)) with a full-width half-maximum (FWHM) bandwidth, which we will abbreviate to bandwidth for the remainder of this paper, of 150 cm^{-1} is shown in Fig. 5(b). The simulation has been shifted in energy to superimpose the experimental spectrum. The simulation is a good reproduction of the experimental spectrum in two respects, namely, the number of vibrational modes that give rise to bands with appreciable intensity and their frequencies. In addition, the relative intensities of the individual members of the ν_{11} progressions are good. However, there is a trend for the ratio of the intensity of the simulation to that of the experimental spectrum to increase slightly as the total energy increases.

Each peak in the PES is notably asymmetric, having a tail to low energy as can be seen from an expansion of the origin band shown in Fig. 6. This is due to the inclusion of numerous unresolved sequence bands in the observed envelope. Therefore, in order to carry out a rigorous simulation of the total PES, we have included all hot bands in our FCF calculations.

A stick spectrum of the calculated wavenumber shifts of the sequence bands associated with the X^2B_1 electronic origin band is also shown in Fig. 6. The first, n = 1, member of each of the most intense ν_N sequence band series, N^1_1, is labelled; n > 1 members are denoted by color-coded asterisks. Other peaks with appreciable intensity are due to combinations of these sequence bands, e.g., the unlabeled peak near −25 cm^{-1} is the $20^1{}_1 30^1{}_1$ band.

A convolution of the stick spectrum with a bandwidth of 150 cm^{-1} shown in the red trace gives a good reproduction of the contour of the experimental peak. All three spectra share a common base line, i.e., there is a count of 5×10^4 at −175 cm^{-1}. Assuming that neither the origin band itself nor its associated sequence bands are broadened by any form of interaction and that the resolution of the spectrometer is ~70 cm^{-1}; this bandwidth yields an unperturbed band contour for ***PhI*** that is ~80 cm^{-1} wide.

It can be seen that the maxima of the experimental peak and its optimized simulation (70 605 cm^{-1}) are offset from the origin of the stick spectrum (70 636 cm^{-1}) as a result of the convolution of all the single vibronic contributions. This offset is confirmed by the fact that the position of the origin of the stick spectrum is in good agreement with that derived from the 1-photon VUV laser-excited MATI spectrum of jet-cooled ***PhI***[12] (70 638 □± 5 cm^{-1}) shown in Fig. 5(b). We will use this approach below to obtain a more accurate value for IE4 for which no MATI spectrum has been recorded.

The MATI spectrum is much cleaner than the PES because of the vibrational and rotational cooling of the sample by the molecular beam and the narrow line width of the excitation laser (~1 cm^{-1}). It can be seen that the observed band intensities in the MATI spectrum are very similar to both the experimental PES and the calculated FCFs; this is to be expected as the MATI intensities are largely determined by FCFs. The MATI technique involves exciting long-lived (>10 μs) Rydberg states that lie a few wave numbers below the ionization limit and then ionizing them using a delayed pulsed electric field. Thus, any process that decreases the lifetime of these Rydberg states will decrease the detection efficiency, and hence the MATI intensities, and this may explain why the intensities of the higher vibronic bands in the MATI spectrum are smaller than in the calculated spectrum.

The MATI spectrum also provides more accurate a_1 vibrational frequencies that can be compared with our calculated values. In addition, many very weak bands, not observable in our spectrum, were assigned[12] to vibrations of different symmetries whose frequencies can also be compared with the calculated values; in almost all cases, the agreement is very good. The data are presented in Table I.

2. The A^2A_2 band

The A^2A_2 band is shown in Fig. 7(b). As in the equivalent band in the PES of the other three mono halobenzenes, the peaks are much broader than those of the X^2B_1 state and only three of them, in addition to the electronic origin, can be identified (see Table III). Our calculations indicate that five vibrational modes, ν_{11}, ν_{10}, ν_9, ν_8, and ν_4, give rise to bands with significant intensity as shown in Fig. 7(a).

Despite the increased number of intense cold bands that were calculated to have appreciable intensity, it was still necessary to increase the bandwidth to 300 cm^{-1} for the optimized simulation of the experimental spectrum shown in Fig. 7(b).

We propose that the increase in bandwidth is due to very rapid IC from the A^2A_2 state vibronic levels to the X^2B_1 state. The nature of the IC will be discussed further in Sec. IV B.We note that the broadening cannot be attributed to predissociation, since the dissociation energy of the ***PhI*** cation ($C_6H_5^+$ + I) is much higher (11.2(1) eV; 90 334 cm^{-1}).[37] As was the case for the X^2B_1 state, the simulation appears to be a reasonable reproduction of the experimental spectrum in terms of the number of vibrational modes that give rise to bands with appreciable intensity and their frequencies. However, there is a greater increase in the ratio of the intensity of the simulation to that of the experimental spectrum as the total energy increases.

3. The B^2B_2 band

B^2B_2 band shown in Fig. 8(b). It can be seen from the stick spectrum in Fig. 8(a) that ν_{10} and ν_9 are the only vibrational modes that are observed; in contrast to the two lower bands, no ν_{11} progressions are observed.

An even greater bandwidth of 400 cm^{-1} is used for the optimized simulation shown in Fig. 8(b), probably as a consequence of the B^2B_2 vibronic levels undergoing IC to both the A^2A_2 andX^2B_1 states. In support of this proposal is the fact that the unresolved 10^1_0 and 9^1_0 peaks in the ***PhI*** spectrum are fully resolved in the equivalent state spectrum of PhBr, as shown in Fig. 2, where the B^2B_2 state is well separated from both of the other two states. In contrast to the two lower states, there is a trend for the ratio of the intensity of the simulation to that of the experimental spectrum to decrease as the total energy increases. The MATI spectrum[12] of the B2B2 state origin of ***PhI*** is a very weak, broad band as shown in Fig. 8(b). This was described as structureless by the authors[12] and although there may be a suggestion of vibronic structure, we do not feel that we can make this assumption. Thus, it appears that both the MATI and PES B^2B_2 state origin bands are ~250 cm^{-1} broader than the equivalent X^2B_1 state origin bands. Kwon et al.[12] equated the B^2B_2 state bandwidth to a lifetime of $<10^{-13}$ s.

In contrast, sharp MATI spectra of the B states of PhBr and PhCl were observed. If the proposed lifetime of the B^2B_2 state of ***PhI*** is correct, it is remarkable that any MATI signal was observed at all and may only be a consequence of the total FC intensity being confined to a single origin band. In contrast, no MATI signal for the A^2A_2 state of ***PhI*** (or PhBr and PhCl) is observed even though we have shown that the PES bands are less broadened. This may be due to the total FC intensity being spread over many vibronic bands in the A^2A_2 state, whereas it is concentrated in the origin of the B^2B_2 state.

4. The C^2B_1 band

This band is shown in Fig. 9(b). The stick spectrum in Fig. 9(a) shows that the spectrum consists of ν_{11} progressions built on the electronic origin, 10^1, 8^1, and 10^2. The ν_{11} vibrational frequency in the C^2B_1 state is smaller than in the ground state of the neutral molecule, whereas the reverse is true for the X^2B_1 state. This effect, together with the fact that a slightly larger bandwidth of 190 cm^{-1} was used in the optimized simulation, cf. 150 cm^{-1} for theX^2B_1 state, explains why the members of the ν_{11} progressions are not as well resolved as in the X^2B_1 state spectrum. The slightly larger bandwidth suggests that the C^2B_1 state is still weakly coupled to one or more of the lower states even though it lies nearly 6000 cm^{-1} above them.

Using the same approach as we applied to the simulation of the experimental origin band of the X^2B_1 state, we obtained a value of 85 035 cm^{-1} for IE_4. In contrast to theX^2B_1 state, this value is the same as the maximum of the experimental peak, i.e., the peak is effectively symmetrical, as shown in the inset in Fig. 9(a).

IV. DISCUSSION

A. Previous simulations of PES

We believe that the present PES simulations are the most extensive ones reported thus far with respect to the size of the molecule and the inclusion of sequence bands. Previously, the largest cations studied were derived from furan, C_5H_4O,[38] and methyl formate, $C_2H_4O_2$,[39] while Huang et al.,[40] included some fundamental hot bands, but not sequence bands, in their study of thiocarbonyl fluoride, F2CS. Most previous attempts to simulate PES have concentrated on the ground ionic state band and, as in the present study, the profile of this band could be accurately simulated.

The study of methyl formate by Nunes et al.[39] had only limited success in simulating the profile of the first excited ionic state. Even though their simulation included a dense manifold of vibronic levels, convolution with the same bandwidth, as was successfully used for the ground state, still produced a structured profile, which contrasts to the experimental spectrum where no structure was observed. As is the case in ***PhI***, the first excited state overlaps the ground state and therefore, the bands of the former are probably broadened by IC; hence, different bandwidths would be required for successful simulations of the two states.

B. Bandwidths in the PES

We have shown that our simulations provide accurate reproductions of the experimental PES in terms of the number of vibrational modes that give rise to bands with appreciable intensity and their frequencies. However, we found it necessary to use different bandwidths in our simulations; 150, 300, 400, and 190 cm−1 for the X2B1, A2A2, B2B2, and C2B1 states, respectively. Kwon et al.[12] observed the same bandwidth, 400 cm−1, for the origin band of the B2B2 state of ***PhI*** in their MATI spectrum and equated it to a lifetime of <10−13 s, where the lifetime refers to the time that the ion remains in its initially populated level before transfer to a dense manifold of levels of a lower state.

We attribute any increase in bandwidth relative to that of theX^2B_1 state to vibronic coupling between an upper state with one or more lower-lying states, using the model described by Baldea et al.[41,42] in an ab initio study on the five lowest ionic states of PhF. They showed that, as might be expected from the values of the IEs, the X^2B_1 and A^2A_2 states are strongly coupled to each other, as are the B^2B_2, C^2B_1, and D^2A_1 states, but that conical intersections between both the X^2B_1 and A^2A_2 potentials and that of the B^2B_2 state had also to be included in a full coupling model. They compared their results with lowresolution PES along with high-resolution MATI and photoinduced Rydberg ionization (PIRI) spectra of the X^2B_1 and C^2B_1 states, respectively. We will reserve a detailed description of their vibronic coupling studies until a later paper[43] on PhF in which we will also present a high-resolution PES for the first time. Crucially, for the current study, Baldea et al.[41,42] proposed that, as a result of vibronic coupling, excitation of an upper state potential above a conical intersection between it and that of a lower state is followed by rapid transfer to the lower surface on the fs timescale. However, they concluded that the transition is not complete and that oscillations of the

populations will be observed and reflect wavepacket motions along several modes of the upper state, resulting in some vibrational structure.

Although we do not directly include vibronic coupling in our simulations, the fact that we have to use different optimized bandwidths for the simulations of different states shows that we are going some way to account for its effect, at least on a semi-empirical basis. Presumably, the different bandwidths required are a consequence of the states having different lifetimes.

Furthermore, the fact that some vibrational structure is observed in, for example, theA^2A_2 band is in line with the weak re-occurrences that Baldea et al.[41,42] predicted in their dynamic simulations on PhF. It is likely that the lifetime of a particular state that is vibronically coupled will decrease with increasing energy and hence, a simulation should ideally include a bandwidth that increases correspondingly. Since we only use a fixed bandwidth for any state, this may explain the increased discrepancy, as energy increases (highlighted above), between the intensities of the simulation and the observed spectrum of a coupled state.

The bandwidth used in the simulation of the C^2B_1 state (190 cm^{-1}) is slightly larger than was used for the X^2B_1 state (150 cm^{-1}) implying that the former is coupled, albeit weakly, to one or more lower states. Baldea et al.[41,42] proposed that an analogous coupling between the X2B1 and B2B2 states in PhF results in transfer from the upper to the lower state via a conical intersection that occurs in a high-energy region of the former, but at a slower rate than for the transfer between the A^2A_2 and X^2B_1 states, that are more strongly coupled, via a conical intersection that is much nearer to their potential minima.

The early phase of PES was primarily directed at arriving at an interpretation of the symmetry sequence of ionic states rather than detailed description of the vibronic manifold. IC is probably widespread in polyatomic ions and is becoming more evident as the resolution of photoelectron spectrometers improves and natural broadening of bands can be distinguished from experimental broadening. Simulations of the type described above also help to distinguish between the two types of broadening. For example, we will show in subsequent papers that IC from the A^2A_2 to the X^2B_1 state also occurs in the other three monohalobenzenes (see also Fig. 2).

C. Lifetimes of ionic and Rydberg states

The lifetimes of an ionic state and, more specifically, the very high-n Rydberg states just below the ionization limit are crucial to the ability to observeMATI spectra of the ionic state, since observation of MATI spectra requires that these high-n Rydberg states are long lived, typically >1 μs. This is almost always true for ground ionic states and the X^2B_1 state MATI spectrum of ***PhI*** is duly observed.12 Although Youn et al.44
did not observe any long-lived excited ionic states of ***PhI***, a very weak, structureless MATI spectrum of the B^2B_2 state was observed,[12] presumably because the lifetime of the state is on the threshold of the crucial value for their observation.
However, long-lived B^2B_2 states of PhBr and PhCl were detected[44] and sharp MATI spectra were observed.[12] No long lived C^2B_1 state of ***PhI*** (or of PhBr and PhCl) was detected[44] although quite narrow vibrational bands are observed in the PES of ***PhI*** and PhBr. No MATI spectra, or any attempts to record them, were reported[12] even though the required VUV laser wavelengths could be generated.

V. Conclusions

The availability of new VUV spectra of the series ***PhX***, includingX = I, which have not been analyzed for the presence of Rydberg states, necessitated a new photoelectron study, which includes vibrational analysis by theoretical means; this PES study of the first four ionic states obtained using synchrotron radiation forms the basis for the current paper. Adiabatic IEs determined using MCSCF procedures confirmed the energy order as: $X^2B_1 < A^2A_2 < B^2B_2 < C^2B_1$. Although it is convenient to retain C_{2v} labelling, there is some evidence that minor distortion to C_S symmetry occurs at the MCSCF level for the C-state. The fifth ionization process shown to be D^2A_1 exhibits dissociation to $C_6H_5^+ + I$, both in the experimental and theoretical studies.
The calculated FC vibrational spectral envelopes for the X^2B_1, A^2A_2, B^2B_2, and C^2B_1 ionic states, including both hot and cold band contributions, reproduce the observed peak positions and intensities with reasonable accuracy. The vibrational analysis shows that many PES individual peaks are summations of several vibrations, and hence more complex than previously thought. Only totally symmetric vibrations give rise to bands with appreciable intensity and these include all modes except C–H stretches.
Our calculations show that hot, sequence band intensities contribute significantly to the observed PES spectral profiles; this is especially convincing for the asymmetric band shapes

in the X^2B_1 state. We found it necessary to use different bandwidths (FWHM) in our simulations, 150, 300, and 400 cm−1 for the X^2B_1, A^2A_2, and B^2B_2, respectively. We believe that the need for larger bandwidths for the A^2A_2 and B^2B_2 states is due to IC from the higher states to the lower one(s). Narrow vibrational structure re-emerges in the second $^2B_1$ band, C2B1 leading to the reduced bandwidth of 190 cm^{-1}, indicating only weak coupling to a lower state. It is likely that the lifetime of a particular state that is vibronically coupled will decrease with increasing energy and hence, a simulation should ideally include a bandwidth that increases correspondingly. Since we only use a fixed bandwidth for any state, this may explain the increased discrepancy, as energy increases, between the intensities of the simulation and the observed spectrum of a coupled state.

The present PES simulations are the most extensive ones reported thus far with respect to the size of the molecule and the inclusion of sequence bands. At this point in time, our calculations do not offer a detailed interpretation of the bandwidths used above for the simulation of the conventional PES; the “best fits” using the values for the bandwidths are purely empirical and pragmatic, since we cannot offer a detailed explanation.

However, we believe the approach used here is of general applicability to other systems and other spectral methods, since the application to MATI spectra is included very successfully. We hope to produce further explanation of the bandwidths following study of other members of the ***PhX*** series which will include new and established REMPI data.

Acknowledgements

We thank: (a) the European Community's Seventh Framework Programme (FP7/2007-2013) CALIPSO under grant agreement nº 312284 for supporting the research leading to these results; (b) the Elettra Synchrotron facility for a Grant of beamtime; (c) the ASTRID2 facility for grants to carry out the parallel VUV absorption study; (d) the NSCCS super-computing facility of the UK for support. MB acknowledges support by the Italian MIUR (under the project PON01-01078/8); MB and AB thank Prof. Vincenzo Barone and Dr. Julien Bloino for helpful discussions.

References

1. M. H. Palmer, T. Ridley, S. Vronning Hoffmann, N. C. Jones, M. Coreno, M. de Simone, C. Grazioli, M. Biczysko, A. Baiardi, and P. Limao-Vieira, J. Chem. Phys. 142, 134302 (2015).
2. M. S. Child, *Theory of Molecular Rydberg States* (Cambridge University Press, Cambridge, 2011).
3. T. F. Gallagher, *Rydberg Ato*ms (Cambridge University Press, Cambridge, 1994).
4. R. S. Mulliken, J. Am. Chem. Soc. 86, 3183 (1964).
5. R. S. Mulliken, J. Am. Chem. Soc. 88, 1849 (1966).
6. M. H. Palmer, S. Vronning Hoffmann, N. C. Jones, A. R. Head, and D. L.Lichtenberger, J. Chem. Phys. 134, 084309 (2011).
7. M. H. Palmer, P. J. Camp, S. Vronning Hoffmann, N. C. Jones, A. R. Head, and D. L. Lichtenberger, J. Chem. Phys. 136, 094310 (2012).
8. M. H. Palmer, S. Vronning Hoffmann, N. C. Jones, E. R. Smith, and D. L. Lichtenberger, J. Chem. Phys. 138, 214317 (2013).
9. J. C. Miller, R. N. Compton, and C. D. Cooper, J. Chem. Phys. 76, 3967 (1982).
10. J. Momigny, C. Goffart, and L. D'Or, Int. J. Mass Spectrom. Ion Phys. 1, 53 (1983).
11. D. M. P. Holland, D. Edvardsson, L. Karlsson, R. Maripuu, K. Siegbahn, A. W. Potts, and W. von Niesson, Chem. Phys. 253, 133 (2000).
12. C. H. Kwon, H. L. Kim, and M. S. Kim, J. Chem. Phys. 116, 10361 (2002).
13. D. M. P. Holland, D. Edvardsson, L. Karlsson, R. Maripuu, K. Siegbahn, A. W. Potts, and W. von Niesson, Chem. Phys. 252, 257 (2000).
14. A. W. Potts, D. Edvardsson, L. Karlsson, D. M. P. Holland, M. A. MacDonald, M. A. Hayes, R. Maripuu, K. Siegbahn, and W. von Niesson, Chem. Phys. 254, 385 (2000).
15. A. M. Gardner and T. G. Wright, J. Chem. Phys. 135, 114305 (2011).
16. K. C. Prince, R. R. Blyth, R. Delaunay, M. Zitnik, J. Krempasky, J. Slezak, R. Camilloni, L. Avaldi, M. Coreno, G. Stefani, C. Furlani, M. de Simone, and M. Stranges, J. Synchrotron Radiat. 5, 565 (1998).
17. N. Martensson, P. Baltzer, P. A. Bruhwiler, J.-O. Forsell, A. Nilsson, A. Stenborg, and B. Wannberg, J. Electron Spectrosc. Relat. Phenom. 70, 117 (1994).
18. D. W. Turner, *Molecular Photoelectron Spectroscopy* (Wiley-Interscience, London, 1970).

19. C. E. Moore, *Ionization Potentials and Ionization Limits Derived from the Analyses of Optical Spectra* (US Govt. Printing Office, Washington DC, 1970).
20. G. C. King, M. Tronc, F. H. Read, and R. C. Bradford, J. Phys. B: At. Mol. Phys. 10, 2479 (1977).
21. See supplementary material at http://dx.doi.org/10.1063/1.4916120 for the following: further details of the PES study; basis sets and CI procedures; ground, excited singlet and ionic structural differences; Franck-Condon ionic state calculated frequencies and intensities.
22. H.-J. Werner, G. K. P. J. Knowles, F. R. Manby, M. Schutz, P. Celani, T. Korona, R. Lindh, A. Mitrushenkov, G. Rauhut, K. R. Shamasundar, T. B. Adler, R. D. Amos, A. Bernhardsson, A. Berning, D. L. Cooper, M. J. O. Deegan, A. J. Dobbyn, F. Eckert, E. Goll, C. Hampel, A. Hesselmann, G. Hetzer, T. Hrenar, G. Jansen, C. Koppl, Y. Liu, A.W. Lloyd, R. A. Mata, A. J. May, S. J. McNicholas,W. Meyer, M. E. Mura, A. Nicklas, D. P. O'Neill, P. Palmieri, K. Pfluger, R. Pitzer, M. Reiher, T. Shiozaki, H. Stoll, A. J. Stone, R. Tarroni, T. Thorsteinsson, M.Wang, and A.Wolf, □□□□□□, version 2012.1, a package of ab initio programs, 2012, see http://www.molpro.net.
23. M. J. Frisch, G. W. Trucks, H. B. Schlegel, G. E. Scuseria, M. A. Robb, J. R. Cheeseman, G. Scalmani, V. Barone, B. Mennucci, G. A. Petersson, H. Nakatsuji, M. Caricato, X. Li, H. P. Hratchian, A. F. Izmaylov, J. Bloino, G. Zheng, J. L. Sonnenberg, M. Hada, M. Ehara, K. Toyota, R. Fukuda, J. Hasegawa, M. Ishida, T. Nakajima,Y. Honda, O. Kitao, H. Nakai, T. Vreven, J. A. Montgomery, Jr., J. E. Peralta, F. Ogliaro, M. Bearpark, J. J. Heyd, E. Brothers, K. N. Kudin, V. N. Staroverov, R. Kobayashi, J. Normand, K. Raghavachari, A. Rendell, J. C. Burant, S. S. Iyengar, J. Tomasi, M. Cossi, N. Rega, J. M. Millam, M. Klene, J. E. Knox, J. B. Cross, V. Bakken, C. Adamo, J. Jaramillo, R. Gomperts, R. E. Stratmann, O. Yazyev, A. J. Austin, R. Cammi, C. Pomelli, J. W. Ochterski, R. L. Martin, K. Morokuma, V. G. Zakrzewski, G. A. Voth, P. Salvador, J. J. Dannenberg, S. Dapprich, A. D. Daniels, O. Farkas, J. B. Foresman, J. V. Ortiz, J. Cioslowski, and D. J. Fox, Gaussian 09, Revision D.01, GAUSSIAN 09, Inc., Wallingford, CT, 2009.
24. V. Barone, J. Bloino, M. Biczysko, and F. Santoro, J. Chem. Theory Comput. 5, 540 (2009).
25. J. Bloino, M. Biczysko, O. Crescenzi, and V. Barone, J. Chem. Phys. 128, 244105 (2008).

26. V. Barone, J. Bloino, and M. Biczysko, Vibrationally-resolved electronic spectra in GAUSSIAN 09, 2009, http://dreamslab.sns.it, accessed November 01, 2014.
27. J. Bloino, M. Biczysko, F. Santoro, andV. Barone, J. Chem. Theory Comput. 6, 1256 (2010).
28. A. Baiardi, J. Bloino, and V. Barone, J. Chem. Theory Comput. 9, 4097 (2013).
29. F. Duschinsky, Acta Physicochim. URSS 7, 551 (1937).
30. V. Barone, J. Chem. Phys. 122, 014108 (2005).
31. V. Barone, M. Biczysko, and J. Bloino, Phys. Chem. Chem. Phys. 16, 1759 (2014).
32. A. J. Sadlej, Theor. Chim. Acta 81, 339 (1992).
33. A. D. McLean and G. S. Chandler, J. Chem. Phys. 72, 5639 (1980).
34. T. H. Dunning, J. Chem. Phys. 90, 1007 (1989).
35. Double and triple-f basis sets of SNS and N07 families are available for download, 2012, http://dreamslab.sns.it (accessed 01.11.2014).
36. I. Carnimeo, C. Puzzarini, N. Tasinato, P. Stoppa, A. P. Charmet, M. Biczysko, C. Cappelli, and V. Barone, J. Chem. Phys. 139, 074310 (2013).
37. Y. Malinovich and C. Lifshitz, J. Phys. Chem. 90, 2200 (1986).
38. S. Bonness, B. Kirtman, M. Huix, A. J. Sanchez, and J. M. Luis, J. Chem. Phys. 125, 014311 (2006).
39. Y. Nunes, G. Martins, N. J. Mason, D. Duflot, S. Vronning Hoffmann, J. Delwiche, M.-J. Hubin-Franskin, and P. Limao-Vieira, Phys. Chem. Chem. Phys. 12, 15734 (2010).
40. C.-H. Huang, C.-C. Chen, Y.-K. Chen, S.-C. Tsai, and J.-P. Chang, Chem. Phys. 440, 99 (2014).
41. I. Baldea, J. Franz, P. G. Szalay, and H. Koppel, Chem. Phys. 329, 65 (2006).
42. E. Gindensperger, I. Baldea, P. G. Szalay, and H. Koppel, Chem. Phys. 338, 207 (2007).
43. M. H. Palmer, T. Ridley, S. Vronning Hoffmann, N. C. Jones, M. Coreno, M. de Simone, C. Grazioli, M. Biczysko, and A. Baiardi, “Combined theoretical and experimental study of the valence, Rydberg and ionic states of fluorobenzene” (unpublished).
44. Y. Y. Youn, C. H. Kwon, J. C. Choe, and M. S. Kim, J. Chem. Phys. 117, 2538 (2002).

Figure Captions

Figure 1. The low-energy region of the PES of ***PhI***, containing the four lowest IEs, which are relevant to the current VUV spectral analysis.

Figure 2. Low-energy region of the PES of the four monohalobenzenes. The intensities of the spectra are normalized to that of the most intense band and are offset on the intensity axis for display purposes.

Figure 3 The electron density contours for the 4 highest occupied MOs of ***PhI.***

Figure 4. Part of the VUV absorption spectra of the four monohalobenzenes. The intensities of the spectra are normalized to that of the most intense band, and are offset on the intensity axis for display purposes. The [3]3s Rydberg states, where [3] indicates a Rydberg state with a third lowest (B) ionic core, have the same relative intensities as the B state bands in the PES.

Figure 5. Stick spectrum of the calculated FCFs for the X^2B_1 band of ***PhI***, (a), in which the color-coded asterisks indicate progressions of $\square_{11}$ built on the electronic origin and the labeled vibrational fundamentals, namely peaks labelled in green indicate transitions to $7^1 11^n$ and peaks labelled in magenta to $4^1 11^n$ excited states. The experimental spectrum is shown in (b) together with a simulation obtained by convoluting the stick spectrum with a bandwidth of 150 cm^{-1}. The simulation is scaled such that the intensity of the origin peak matches that of the experimental spectrum. The 1-photon MATI spectrum,[12] with intensity scaled to match the PES origin and offset for display purposes, is also show in (b).

Figure 6. Stick spectrum of the calculated wavenumber shifts of the sequence bands associated with the X^2B_1 electronic origin peak (lower black trace). The first, $n = 1$, member of a $\square_N$ sequence band series, N^1_1 is labelled; $n > 1$ members are denoted by color-coded asterisks. A convolution of this spectrum with a bandwidth of 150 cm^{-1} is shown in the red trace while the upper black trace shows the experimental band appropriately offset in energy.

Figure 7. Stick spectrum of the calculated FCFs for the A^2A_2, band, (a), in which the color-coded asterisks indicate progressions of $\square_{11}$ built on the electronic origin and the labeled vibrational fundamentals. The experimental spectrum is shown in (b) together with a simulation obtained by convoluting the stick spectrum with a bandwidth of 300 cm^{-1}. The simulation is scaled such that the intensity of the origin peak matches that of the experimental spectrum.

Figure 8. Stick spectrum of the calculated FCFs for the B^2B_2 band, (a). The experimental spectrum is shown in (b) together with a simulation obtained by convoluting the stick

spectrum with a bandwidth of 400 cm^{-1}. The 1-photon MATI spectrum,[12] with intensity scaled to match the PES origin and offset for display purposes, is also shown in (b).

Figure 9. Stick spectrum of the calculated FCFs for the C^2B_1 band, (a). The experimental spectrum is shown in (b) together with a simulation obtained by convoluting the stick spectrum with a bandwidth of 190 cm^{-1}. An expansion of the origin band, offset in energy, is shown in the inset in (a).

Table I. Experimental frequencies for the vibrational modes, numbered according to the Mulliken convention, of the ground states of neutral and ionic ***PhI*** together with calculated anharmonic values for various states of the ion. All values in cm^{-1}.

		Neutral		Ion				
		Ground		X^2B_1		A^2A_2	B^2B_2	C^2B_1
Mode	Symmetry	Exp.[a]	Calc.	Calc.	Exp.[b]	Calc.	Calc.	Mode
1	a_1	3064	3089	3099		3105	3227[c]	3249[c]
2		3050	3088	3096		3082	3203[c]	3226[c]
3		3031	3009	3035		3040	3159	3175
4		1575	1613	1596	1575	1561	1687	1763
5		1473	1504	1469		1521	1591	1588
6		1178	1200	1213		1207	1272	1301[d]
7		1060	1081	1060	1036	1105	1111	1093
8		1015	1039	1018[c]	1015	1028	1073[c]	1049
9		998	1022	1004[c]	990	994	1027[c]	1036
10		654	675	679	661	668	670	671
11		266	271	290	284	276	248	234
12	a_2	963	994	1018		1008	1076	1060
13		835	849	822		862	897	900
14		398	410	363	357	298	423	434
15	b_1	987	1003	1020		1005	1100	1042
16		904	927	968	903	898	1002	1009
17		730	742	762	808	712[c]	793	800
18		684	687	604		380	695	709
19		448	462	409	406	365[c]	467	502
20		181	154	124	127	130	158	158
21	b_2	3064	3098	3110		3097	3227[c]	3246
22		3048	3071	3093		3085	3210[c]	3225
23		1575	1612	1524[c]	1517	2048	1716	1643
24		1435	1467	1424[c]		1424	1562	1502
25		1321	1344	1363[c]		1366	1440	1440
26		1261	1274	1292[c]		1349	1301[c]	1280[d]
27		1159	1175	1172		1218	1174[c]	1156
28		1068	1083	1097		964	1139	1145
29		613	631	574	538	654	650	658
30		220	224	229	242	219	198	200

[a] Reference 15.
[b] Reference 12.
[c] Upper state normal coordinate is made up of a significant mixing of two neutral ground state normal coordinates of the same symmetry in C_{2v}.
[d] Upper state normal coordinate is made up of a significant mixing of two neutral ground state normal coordinates of different symmetries in C_{2v}.

Table II. The experimental adiabatic ionization energies IE_1 to IE_4 for ***PhI*** together with those calculated using UB3LYP and MCSCF. Vertical IEs and pole strengths calculated using GF procedures are numerically close to experiment, indicating that relatively small changes occur for each ionic state.

Exp. IE / eV	GF calc. vertical IE / eV	Pole strength	UB3LYP calc. adiabatic IE / eV	MCSCF calc. adiabatic IE / eV	Leading term vacancy	Calc. state symmetry
8.758	8.669	0.902	8.530	7.741	$3b_1^{-1}$	X^2B_1
9.505	9.466	0.890	9.289	8.015	$1a_2^{-1}$	A^2A_2
9.776	9.621	0.912	9.683	8.697	$6b_2^{-1}$	B^2B_2
10.543	10.497	0.894	10.715	9.729	$2b_1^{-1}$	C^2B_1

Table III. Observed peak positions in the PES of ***PhI***, shifts from the origin of the vibronic bands, their assignments and calculated fundamental vibrational ionic frequencies of the modes observed.

Peak position / eV	Shift from origin / eV	Peak position / cm^{-1}	Shift from origin / cm^{-1}	Calc. fundamental frequency / cm^{-1}	Major Assignment
X^2B_1					
8.691	-0.063	70 097	−508		11_2
8.722	-0.032	70 347	−258		11_1
8.754	0	70 605	0		0^0
8.789	0.035	70 887	282	290	11^1
8.824	0.070	71 170	565		11^2
8.857	0.103	71 436	831		11^3
8.882	0.128	71 637	1032	1060+1004	7^1+9^1
8.914	0.160	71 895	1290		$7^111^1+9^111^1$
8.948	0.194	72 170	1565	1596	$4^1+7^111^2$
8.980	0.226	72 428	1823		$4^111^1+7^111^3$
A^2A_2					
9.505	0	76 663	0	276	0^0+11^1
9.575	0.070	77 227	565	668	10^1
9.633	0.128	77 694	1032	1028+994	8^1+9^1
9.703	0.198	78 259	1560	1561	4^1
B^2B_2					
9.776	0	78 848	0		0^0
9.872	0.096	79 622	774	669+1027	9^1+10^1
9.938	0.162	80 155	1307		10^1
9.990	0.214	80 574	1726		9^110^1
C^2B_1					
10.511	-0.032	84 776	-258		11_1
10.543	0	85 035	0		0^0
10.569	0.026	85 244	210	234	11^1
10.594	0.051	85 445	411		11^2
10.621	0.078	85 664	629	671	10^1
10.645	0.102	85 857	823		10^111^1

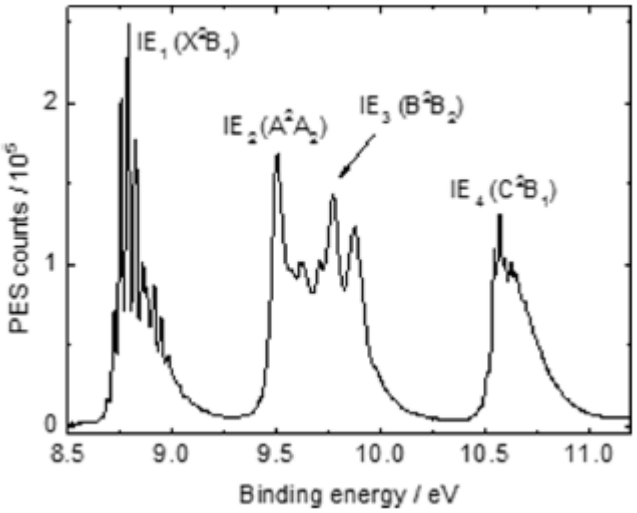
IE1 (X2B1)
IE2 (A2A2)
IE3 (B2B2)
IE4 (C2B1)
PES counts / 10^5
Binding energy / eV

Fig. 1

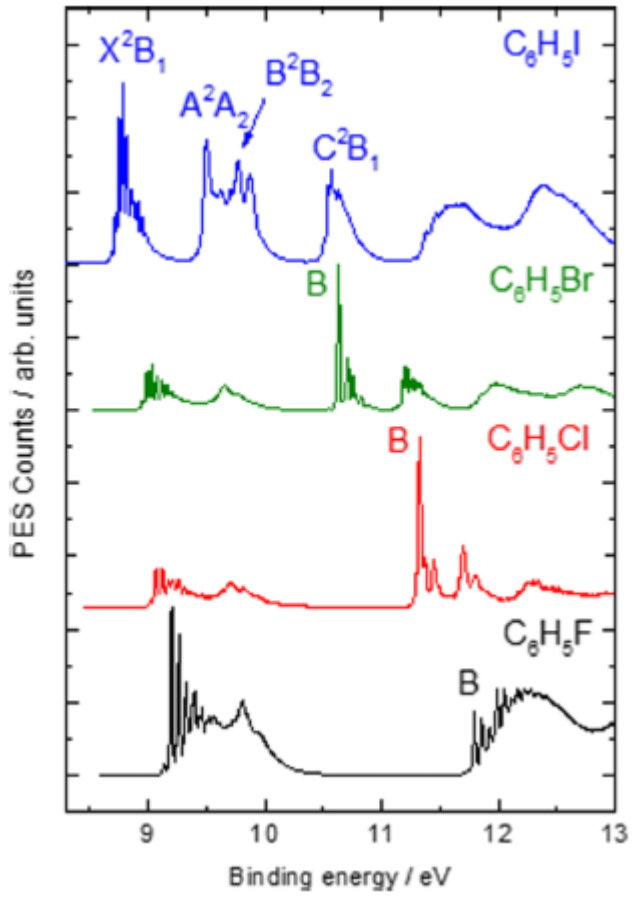
X2B1
A2A2
B2B2
C2B1
C6H5I
B
C6H5Br
B
C6H5Cl
C6H5F
B
PES Counts / arb. units
Binding energy / eV

Fig. 2

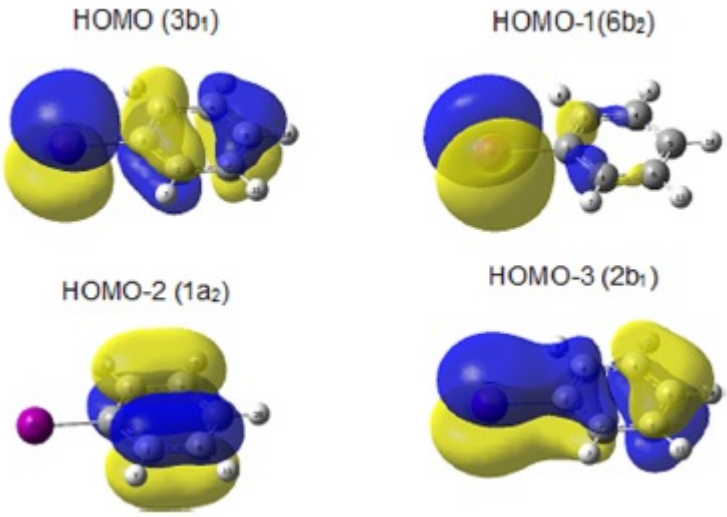
HOMO (3b1)
HOMO-1(6b2)
HOMO-2 (1a2)
HOMO-3 (2b1)

Fig. 3

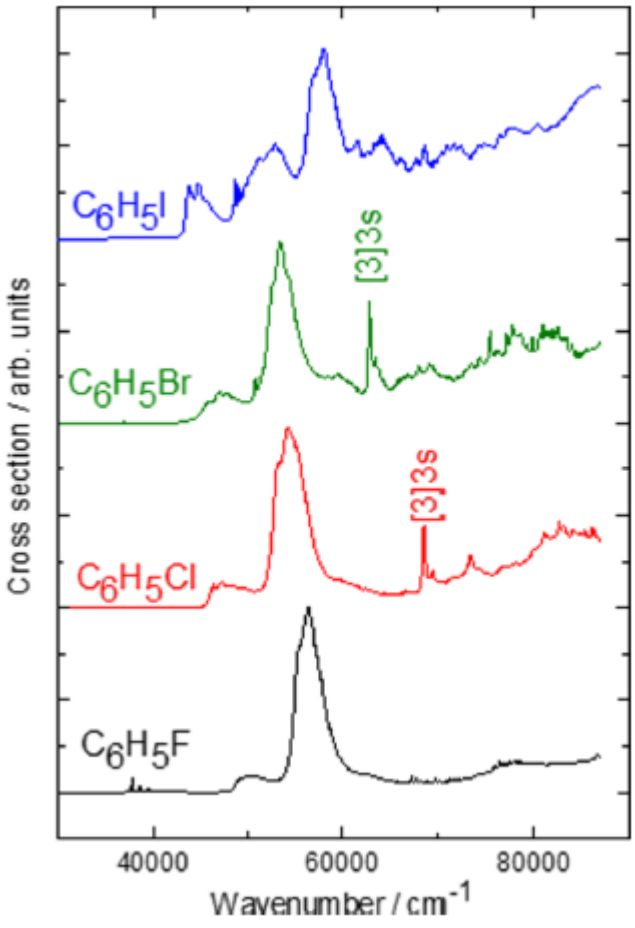
C6H5I
C6H5Br
C6H5Cl
C6H5F
[3]3s
[3]3s
Cross section / arb. units
40000
60000
80000
Wavenumber / cm-1

Fig. 4

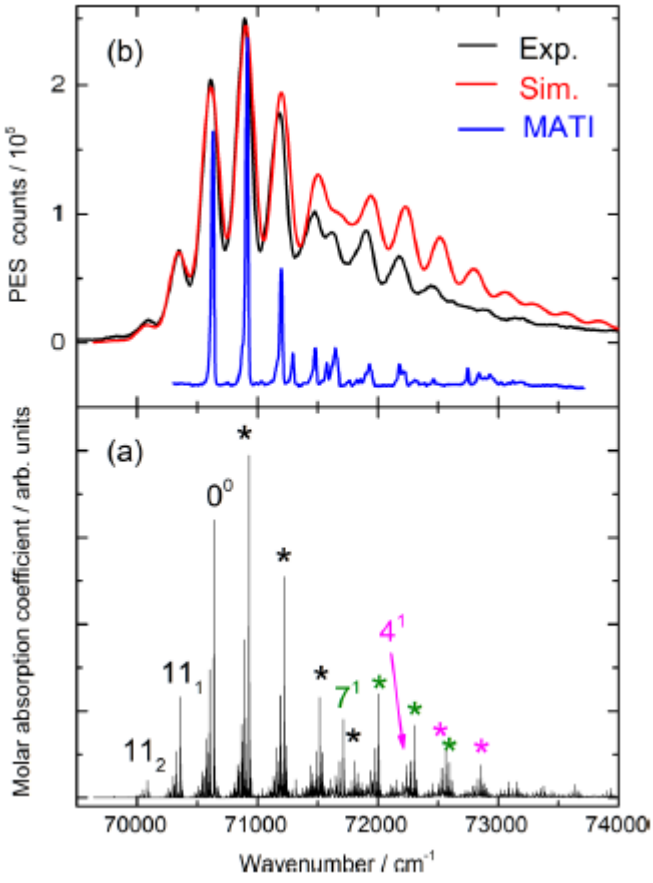
(b)
Exp.
Sim.
MATI
PES counts / 10^5
(a)
0^0
11_1
11_2
7^1
4^1
Molar absorption coefficient / arb. units
70000
71000
72000
73000
74000
Wavenumber / cm^-1

Fig. 5

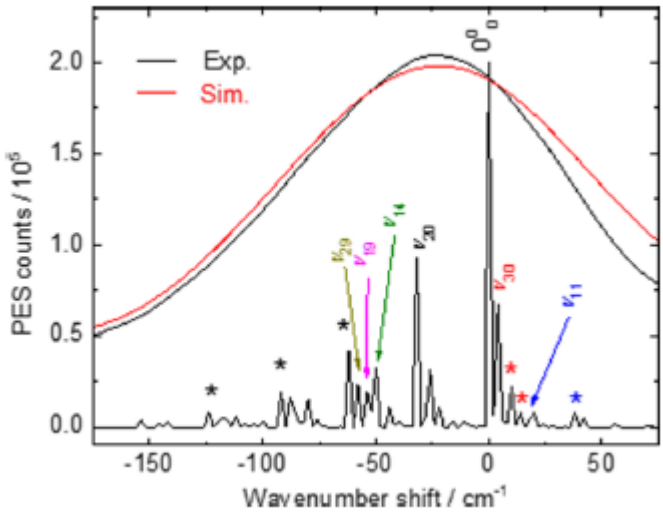
Exp.
Sim.
0^0_0
PES counts / 10^6
Wavenumber shift / cm^-1

Fig. 6

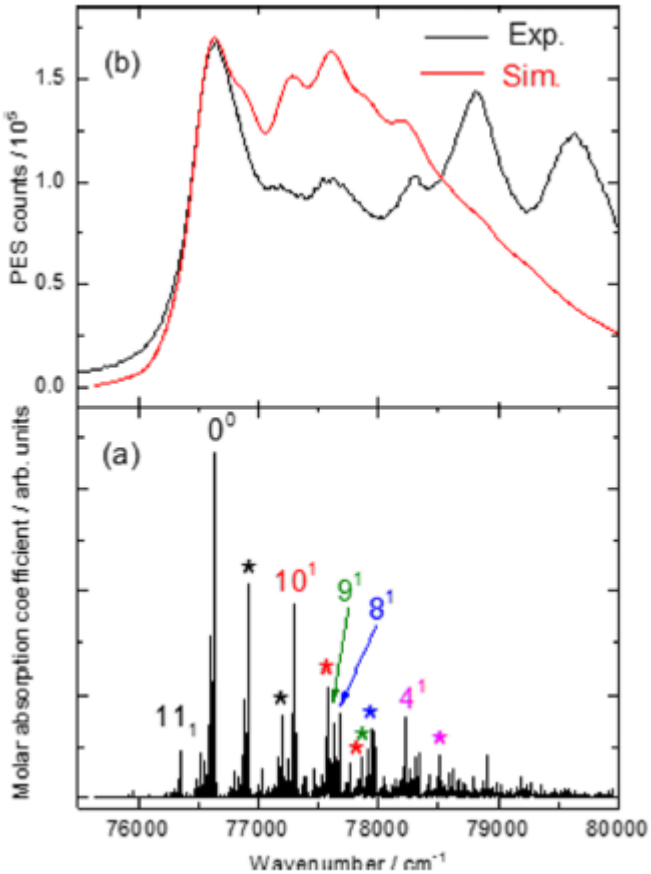
(b)
Exp.
Sim.
PES counts / 10^5
1.5
1.0
0.5
0.0
(a)
0^0
10^1
9^1
8^1
4^1
11_1
Molar absorption coefficient / arb. units
76000
77000
78000
79000
80000
Wavenumber / cm^-1

Fig. 7

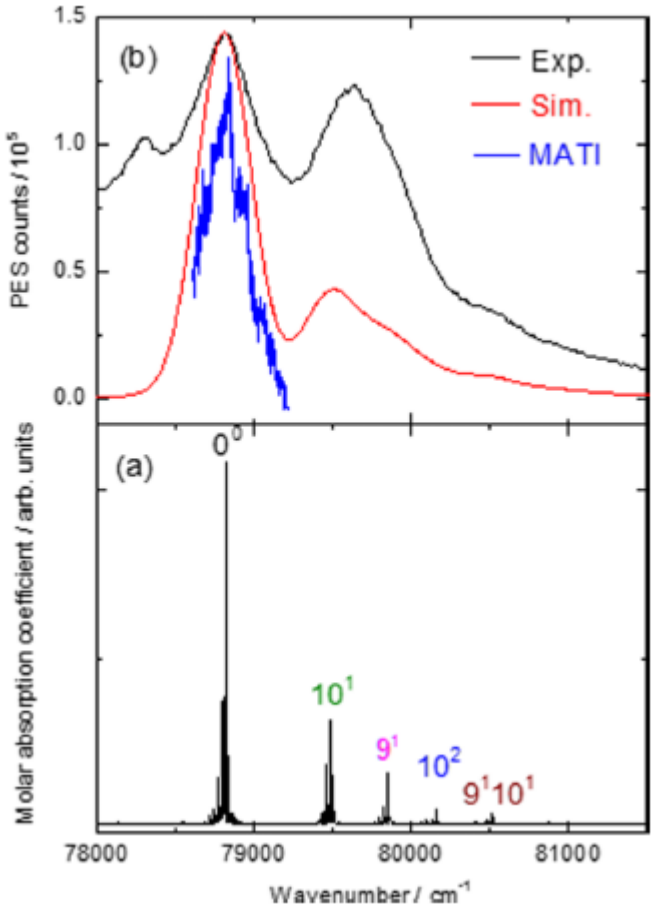
(b)
Exp.
Sim.
MATI
PES counts / 10^5
1.5
1.0
0.5
0.0
(a)
0^0
10^1
9^1
10^2
9^110^1
Molar absorption coefficient / arb. units
78000
79000
80000
81000
Wavenumber / cm^-1

Fig. 8

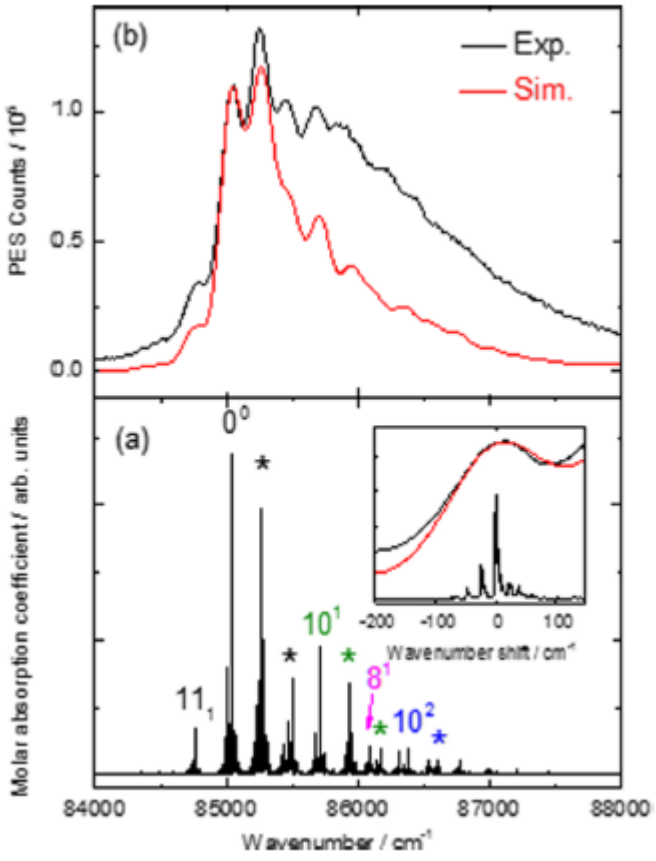
(b)
Exp.
Sim.
PES Counts / 10⁶
1.0
0.5
0.0
(a)
0⁰
10¹
11₁
8¹
10²
-200
-100
0
100
Wavenumber shift / cm⁻¹
Molar absorption coefficient / arb. units
84000
85000
86000
87000
88000
Wavenumber / cm⁻¹

Fig. 9